XVII IMEKO World Congress
Metrology in the 3rd Millennium
June 22–27, 2003, Dubrovnik, Croatia

THE EFFECT OF DIFFERENT INLET - VELOCITY PROFILES ON THE PERFORMANCE OF A CORIOLIS FLOWMETER

Gregor Bobovnik, Jože Kutin, Ivan Bajsić

University of Ljubljana, Faculty of Mechanical Engineering, Ljubljana, Slovenia

Abstract – Numerical simulations (using finite volume method) of the flow of a viscous fluid through a measuring tube were performed to identify the effects of different inlet-flow conditions on the performance of a straight, slender-tube, Coriolis flowmeter. The magnitudes of the anti-symmetric fluid forces and the twisting moments acting on the measuring tube were compared with results from a one-dimensional fluid-flow model. Simulations were made for some hypothetical inlet-velocity profiles that represent extreme cases of various flowmeters' installation positions and flow regimes in a pipeline. No significant effects of the modelled inlet-velocity profiles on the performance of the flowmeter were observed.

Keywords: Coriolis flowmeter, velocity profile, numerical simulation.

1. INTRODUCTION

The primary sensing element of a Coriolis flowmeter is a measuring tube that conveys fluid and is maintained vibrating at its natural frequency. The fluid that flows in the vibrating tube is subjected to the Coriolis force, the magnitude of which is proportional to the product of the fluid's mass flow rate and the local angular velocity of the vibrating tube. Due to the Coriolis force the tube's mode shape becomes anti-symmetric, the effect which is exploited as the basic measuring principle.

The installation effects – including the influence of pulsating and two-phase flows, the effects of fluid pressure, fluid temperature and the external vibrations – on the performance of flowmeters have already been thoroughly studied, but very few attempts have been made to determine the effects of the inlet-flow conditions.

Durst and Raszillier [1] studied fully developed flow in a tube rotating around an axis perpendicular to its own. The existence of secondary flow, which occurs in a rotating tube, is also predicted for the vibrating measuring tube, where it might be an additional source of anti-symmetry in the tube oscillation.

Cheesewright, Clark and Bisset [2] experimentally investigated the effects of swirl and velocity-profile asymmetry in the inlet flow. Flow disturbances were introduced by the insertion of partial blockage plates at the upstream flange (asymmetry) and a helically twisted strip (swirl) in the upstream spool pipe. Tests were carried out for three different types of commercial flowmeter, and no, or only small changes in the flowmeter's calibration were observed.

Hemp [3] applied the weight vector theory to a simple flowmeter configuration consisting of an unsupported straight tube unattached to adjacent piping. He showed that the sensitivity of a flowmeter depends, in part, on interaction of the velocity profile with the fluid vibration near the ends of the tube. When these end effects are taken into account the flowmeter reads lower than it would do if the end effects are ignored. Because of the end effect an increase in the sensitivity is predicted for turbulent flow.

In this article the effects of inlet-velocity profiles on the performance of a straight, slender-tube, Coriolis flowmeter were studied using the commercially available Comet code [4], which is based on finite volume method. The velocity and pressure fields in the tube, as well as the magnitudes and the distribution of fluid forces exerted on the tube, were investigated. The twisting moment that causes an additional deflection of the tube's mode shape was calculated from the fluid force distribution. The comparison of numerical values (the magnitudes of the resulting force and the twisting moment) with those obtained using the one-dimensional model led to a prediction of the inlet-velocity profile's effect on the sensitivity of the flowmeter.

2. THE ONE-DIMENSIONAL MODEL

We used a model based on the Euler beam theory and a one-dimensional flow field to evaluate the data obtained from the numerical simulation. If we consider a measuring tube with flexural rigidity EI, mass per unit length M, and denote the tube's longitudinal axis by x, the time by t, the lateral deflection of the tube by $w(x,t)$, the mass of fluid per unit length by M_f and the uniform fluid velocity in the tube by V, the equation of motion is expressed as follows:

$$EI\frac{\partial^4 w}{\partial x^4}+M\frac{\partial^2 w}{\partial t^2}=-M_f V^2\frac{\partial^2 w}{\partial x^2}-2M_f V\frac{\partial^2 w}{\partial x\partial t}-M_f\frac{\partial^2 w}{\partial t^2}. \quad (1)$$

The effects of added masses, external forces, damping, pressure and excitation forces were neglected. The terms on the left-hand side of (1) represent the tube's stiffness and inertia, these are independent of flow and so describe a simple transversal vibration of the measuring tube. The terms on the right-hand side of (1), from left to right, represent the relative centrifugal, the Coriolis and the

inertial translational forces, respectively, resulting from the presence of fluid flow in a vibrating tube.

The first mode shape $W_1(x)$ of the lateral vibration of the measuring tube, with fixed ends of length L, in the absence of the fluid flow, is obtained from the left-hand side of (1) and has the following form [5]:

$$W_1(x) = C_1 F_1(x) = C_1 \left[\cosh\left(\lambda_1 \frac{x}{L}\right) - \cos\left(\lambda_1 \frac{x}{L}\right) - \frac{\cosh\lambda_1 - \cos\lambda_1}{\sinh\lambda_1 - \sin\lambda_1} \left(\sinh\left(\lambda_1 \frac{x}{L}\right) - \sin\left(\lambda_1 \frac{x}{L}\right) \right) \right], \quad (2)$$

where λ_1 is the coefficient that determines the first mode shape and C_1 is the factor that defines the amplitude of the vibration. In our case $\lambda_1 = 4{,}730$ and $C_1 = A/F_1(L/2)$ and A defines the amplitude of vibration in the middle of the tube.

The deflection of the tube's mode shape cannot be obtained with a numerical simulation; only the pressure and the velocity field in the measuring tube are calculated (fluid domain). During the simulation (presented in the next section), the shape of the fluid's computational domain is therefore modified according to the first mode shape of the measuring tube (2).

For the prescribed mode shape (2) the Coriolis effect, which is correlated with the anti-symmetric deflection of the tube's mode shape, is most easily estimated from the difference between the magnitudes of the resulting Coriolis forces on the tube's left and right halves ($R_{a,y}$):

$$R_{a,y} = -2M_f V\omega \left(\int_{L/2}^{L} \frac{\mathrm{d}W_1}{\mathrm{d}x}\mathrm{d}x - \int_{0}^{L/2} \frac{\mathrm{d}W_1}{\mathrm{d}x}\mathrm{d}x \right) = 4M_f V\omega A, \quad (3)$$

where ω is the circular frequency of the tube.

A more precise estimation of the Coriolis effect is expected by defining the twisting moment, M_a, around the middle of the tube, because the value of the moment contains information relating to the force distribution along the tube's length, and not just its magnitude. For determining the magnitude of the twisting moment, only the Coriolis force, for its anti-symmetry in the middle position of the tube, has to be taken into account:

$$M_a = 2 \cdot \left[-2M_f V\omega \int_0^{L/2} \frac{\mathrm{d}W_1}{\mathrm{d}x} \left(\frac{L}{2} - x \right) \mathrm{d}x \right] = 8 \frac{M_f V\omega C_1 L}{\lambda_1} \frac{\cosh\lambda_1 - \cos\lambda_1}{\sinh\lambda_1 - \sin\lambda_1}. \quad (4)$$

3. NUMERICAL MODEL

Numerical simulations were performed using the Comet code, which is based on the finite volume discretization method. This section presents the numerical grid that was used in the simulations, the mathematical model that was incorporated in the code, the initial and boundary conditions of the simulations and the calculation of the resulting force difference, $R_{n,y}$, and the twisting moment, M_n.

3.1. Discretization of the computational domain

The computational domain consists of the measuring tube, and the inlet and outlet piping sections, the dimensions of which are presented (with respect to D) in Fig. 1. The inner diameter D for all the sections is equal to 0,01 m.

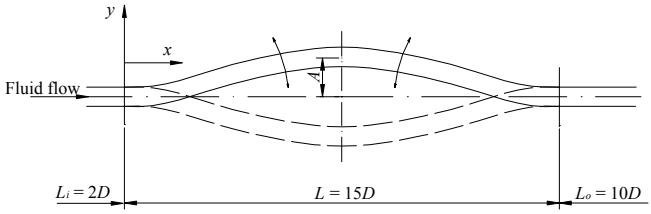

Fig. 1. Scheme of the computational domain

The numerical grid used in the simulations consisted of 73340 cells (finite volumes). The cells representing the measuring tube were uniformly distributed in the axial direction, while the distances between the centres of the cells in the inlet (outlet) region are increased by a factor 1,03 towards the beginning (end). Number of cells of the numerical grid is listed in Table I.

The appropriate numerical grid was selected after a comparison of the results obtained on three different grids (the first was 1,3-times coarser and the second 1,4-times denser, than the selected one). The values of the fluid forces and of the twisting moment were compared. For all three grids the compared values deviated by less than 0,1 %.

TABLE I. Number of cells of the selected numerical grid

Total	73340
In cross-section	380
In the axial direction	180
- Measuring tube	150
- Inlet	8
- Outlet	35

3.2. Mathematical model

The basic equations used for the description of fluid flow in Comet are presented in this section. The model is presented for isothermal and incompressible fluid flow. For a fluid with density ρ, fluid velocity vector $\mathbf{v}$, and surface velocity (of the finite volume) $\mathbf{v}_s$, the continuity and momentum equations are:

$$\frac{\partial}{\partial t}\int_V \rho \mathrm{d}V + \int_S \rho(\mathbf{v} - \mathbf{v}_s)\mathrm{d}\mathbf{s} = 0 \quad (5)$$

and

$$\frac{\partial}{\partial t}\int_V \rho\mathbf{v}\mathrm{d}V + \int_S \rho\mathbf{v}(\mathbf{v} - \mathbf{v}_s)\cdot\mathrm{d}\mathbf{s} = \int_S \mathbf{T}\cdot\mathrm{d}\mathbf{s} + \int_V \mathbf{f}_b \mathrm{d}V, \quad (6)$$

where $\mathbf{f}_b$ represents the vector of forces acting on the fluid volume and $\mathbf{T}$ is the strain tensor, which is defined as:

$$\mathbf{T} = 2\mu_e \dot{\mathbf{D}} - \frac{2}{3}\mu_e \operatorname{div}\mathbf{v}\,\mathbf{I} - \left(p + \frac{2}{3}(\mu_t \operatorname{div}\mathbf{v} + \rho k) \right)\mathbf{I}, \quad (7)$$

where

$$\dot{\mathbf{D}} = \frac{1}{2}\left(\operatorname{grad}\mathbf{v} + (\operatorname{grad}\mathbf{v})^T\right) \tag{8}$$

is the rate of the strain tensor, p is the pressure, $\mathbf{I}$ is the unit tensor and μ_e is the effective viscosity of the fluid defined as the sum of the dynamic μ and the turbulent μ_t viscosities:

$$\mu_e = \mu + \mu_t \tag{9}$$

The turbulent viscosity is obtained by using the standard k-ε model:

$$\mu_t = C_\mu \rho \frac{k^2}{\varepsilon}, \tag{10}$$

where k is the kinetic energy of the turbulence and ε is its dissipation rate. Their values are obtained by solving their respective transport equations:

$$\begin{aligned}\frac{\partial}{\partial t}\int_V \rho k \mathrm{d}V + \int_S \rho k(\mathbf{v}-\mathbf{v}_s)\mathrm{d}\mathbf{s} &= \int_S \left[\left(\mu + \frac{\mu_t}{\sigma_k}\right)\operatorname{grad} k\right]\mathrm{d}\mathbf{s} \\ &+ \int_V \left(2\mu_t \dot{\mathbf{D}} : \dot{\mathbf{D}} - \frac{2}{3}(\mu_t \operatorname{div}\mathbf{v} + \rho k)\operatorname{div}\mathbf{v} - \rho\varepsilon\right)\mathrm{d}V\end{aligned} \tag{11}$$

$$\begin{aligned}\frac{\partial}{\partial t}\int_V \rho \varepsilon \mathrm{d}V + \int_S \rho\varepsilon(\mathbf{v}-\mathbf{v}_s)\mathrm{d}\mathbf{s} &= \int_S \left[\left(\mu + \frac{\mu_t}{\sigma_\varepsilon}\right)\operatorname{grad}\varepsilon\right]\mathrm{d}\mathbf{s} \\ &+ \int_V \left(C_1 P\frac{\varepsilon}{k} - C_2\rho\frac{\varepsilon^2}{k} + C_3\rho\varepsilon\operatorname{div}\mathbf{v}\right)\mathrm{d}V.\end{aligned} \tag{12}$$

The quantities C_μ C_1, C_2, C_3, σ_k and σ_ε are empirical factors. Their values are given in Table II.

For simulations at Re = 400 the turbulence was not modelled, which means that the values of μ_t is equal to 0.

TABLE II. Values of empirical factors used in the standard k-ε turbulence model

C_μ	C_1	C_2	C_3	σ_k	σ_ε
0,09	1,44	1,92	-0,33	1,0	1,3

3.3 Initial and boundary conditions

The first mode shape of the fixed-fixed Euler beam was used to model the vibration of the tube. By taking into account the expression in (2) a lateral deflection of the tube with respect to the coordinate x and the time t can be written as:

$$w_1(x,t) = W_1(x)\cos(\omega t) \tag{13}$$

The amplitude of vibration in the middle of the tube (A) was equal to L/300. The vibration of the tube was simulated using the moving-grid option, which starts when the fluid flow in the tube reaches its steady state. A single period is modelled with 130 time steps. The numerical results obtained were always observed when the periodic regime of the flow in the vibrating measuring tube was reached, this is because the transient regime is of no importance for mass flow measurements.

Fig. 2 shows the hypothetical inlet velocity profiles that may occur as a result of various installation positions of the flowmeter. Each profile is denoted with a letter written next to its name in the legend of Fig. 2. In the case of the triangular and the uniform-velocity profiles, swirl was also introduced on the inlet (these simulations are marked with the letter S). The circumferential swirl velocity in the inlet cross-section is defined as:

$$v_v(r) = \alpha V \frac{r}{R}, \tag{14}$$

where the coefficient α represents the ratio between the maximum swirl velocity and the average axial velocity, V, and the ratio r/R is the dimensionless radial position. The coefficient α was taken to be 0,1 and 0,25, respectively. In addition to these profiles, fully developed laminar and turbulent velocity profiles (marked with the letter D in the reminder of the text), were also used as inlet boundary conditions. Fully developed velocity profiles were obtained from a preliminary simulation of fluid flow in the tube at rest.

The simulations were made for Re = 400 and 20000, using the tube vibrating frequency of 100 Hz.

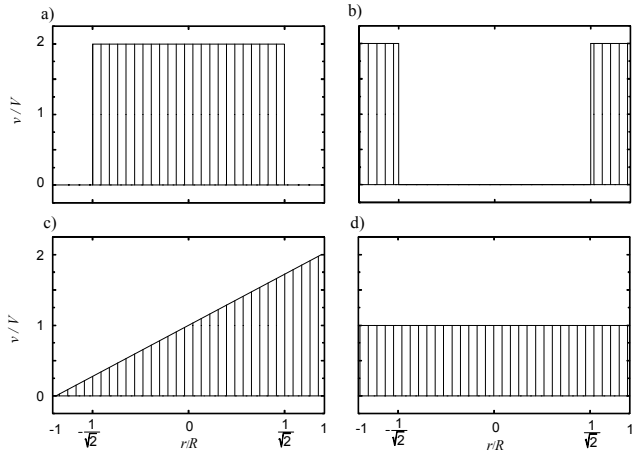

Fig. 2. Inlet-velocity profiles: a) with increased velocity in the middle - C, b) with increased velocity near the walls - W, c) triangular - T, d) uniform - U

3.4. Evaluation of the fluid forces and the twisting moment

The fluid forces acting on the tube's wall are calculated from the pressure field that results from the numerical simulation. As was mentioned at the beginning of this section, the measuring tube is divided in the axial and circumferential directions. So the idea is first to sum up the forces acting on the boundary elements of a single ring (which results from axial discretization of the tube) and then to sum up the forces acting on the rings of the measuring tube.

The force acting on the boundary element k in the direction of the y-axis can be written as a sum of the friction $T_{k,y}$ and the pressure forces $p_k s_{k,y}$, where $s_{k,y}$ is the component y of the surface vector of the boundary k:

$$F_{k,y} = T_{k,y} + p_k s_{k,y}. \tag{15}$$

From summing up the forces acting on the boundary surfaces of a particular ring the force acting on the ring *j* is:

$$F_{j,y} = \sum_{k \in j} F_{k,y} \,. \tag{16}$$

The Coriolis effect can then be then estimated from the difference between the forces acting in the direction of the *y*-axis on the tube's left and right halves. Assuming that the measuring tube is divided into *N* equally-wide sections, the resulting difference, R_y, equals (Fig. 3):

$$R_y = \sum_{j=\frac{N}{2}+1}^{N} F_{j,y} - \sum_{j=1}^{\frac{N}{2}} F_{j,y} \tag{17}$$

The value R_y is calculated for each time position of the measuring tube. Theoretically, we could determine the magnitude of the force difference in (17) by calculating its value in the middle position of the tube, where the Coriolis force (as the only anti-symmetric force) reaches its maximum value. Because the oscillation of the tube is modelled with a finite number of time steps, we cannot exactly follow the tube motion in time, so we approximate the set of values from (17) for a single oscillation with:

$$R_y(t) = R_{n,y} \sin(2\pi f t - \phi), \tag{18}$$

where R_{ny} is the amplitude of the resulting force difference, *f* is the vibrating frequency of the tube and ϕ is the phase angle.

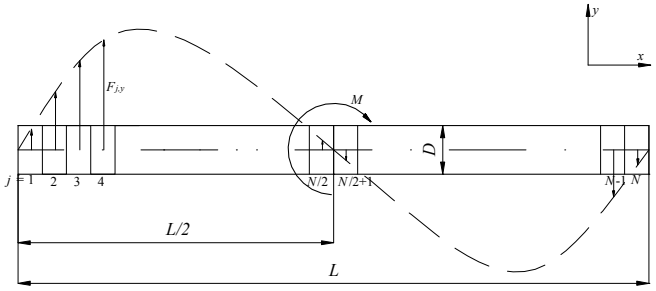

Fig 3. Calculation of the twisting moment

If we consider that the force acts in the middle of the ring's width, and that the measuring tube is divided equidistantly, the twisting moment that acts around the middle of the tube (Fig. 3) is calculated as:

$$M = \sum_{j=1}^{N} F_{j,y} \left(\frac{L}{2} - \left(j - \frac{1}{2} \right) \cdot \frac{L}{N} \right), \tag{19}$$

where L/N represents the width of a single ring. To determine its magnitude, M_n, the same approximation as in (18) is used:

$$M(t) = M_n \sin(2\pi f t - \phi). \tag{20}$$

4. RESULTS

In this section we compare the numerical results and the results from the analytical model. The magnitudes of the resulting forces obtained from (3) and (18), and the magnitudes of the twisting moments from (4) and (20) were compared. The agreement between the numerically and analytically obtained values was defined as:

$$u_R = \frac{R_{n,y}}{R_{a,y}} \text{ and } u_M = \frac{M_n}{M_a}. \tag{21}$$

If u_R and u_M are equal to 1 then the numerical and analytical values are the same.

The agreement of the magnitudes of the resulting force u_R is presented in Fig. 4 for Reynolds numbers 400 and 20000. It is clear that all the simulations are in relatively good agreement with the assumption of the one-dimensional model. No significant difference between the various inlet profiles at constant *Re* is observed, although the values of agreement from (21) of numerical results for *Re* = 400 are significantly smaller than for *Re* = 20000.

The agreement of values of the twisting moment magnitude, u_M, in Fig. 5 has practically the same characteristics as u_R in Fig. 4. On this basis we can claim that the comparison of the twisting moment values does not give any new information, which means that not only are the amplitudes of the fluid forces acting on the tube's wall the same, but also that the fluid force distribution obtained numerically might be in very good agreement with the analytically predicted one. We have also established that the measuring effect is slightly affected by the different Reynolds numbers, but it seems that the inlet-velocity profiles do not have any characteristic influence on the flowmeter's performance.

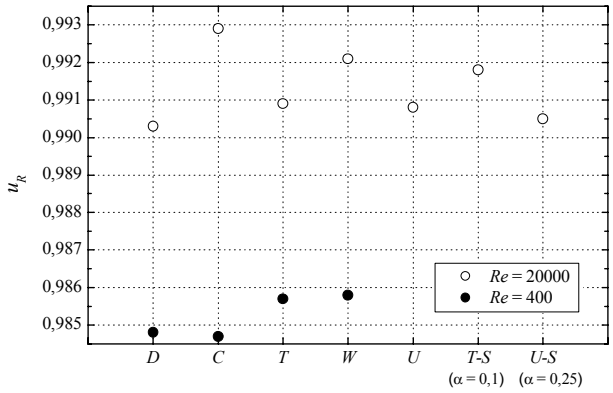

Fig. 4. Agreement of the magnitudes of the resulting force

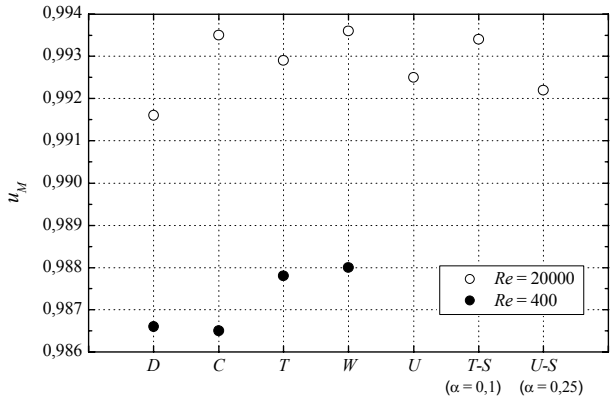

Fig. 5. Agreement of the magnitudes of the twisting moment

5. CONCLUSION

Simulations of the flow of a fluid through the measuring tube of a Coriolis flowmeter were made for various inlet-velocity profiles. Numerically obtained values of the fluid forces and the twisting moment magnitudes that act on the measuring tube were further compared with values obtained from a one-dimensional model. From the comparisons made we can conclude that the various inlet profiles, which were in our case hypothetical, do not have any significant influence on the flowmeter's performance. The results show that the sensitivity of the flowmeter might decrease, with respect to the linear characteristics predicted by the one-dimensional model, in the region of lower Reynolds numbers.

REFERENCES

[1] F. Durst, H. Raszillier, "Flow in a Rotating Straight Pipe, with View on Coriolis Mass Flow Meter", *Journal of Fluids Engineering*, vol. 112, pp. 149 – 154, 1990.

[2] R. Cheesewright, C. Clark, D. Bisset, "The Identification of External Factors which Influence the Calibration of Coriolis Massflow Meters", *Flow Measurement and Instrumentation*, vol. 11, pp. 1 – 10, 2000.

[3] J. Hemp, "Calculation of the Sensitivity of a Straight Tube Coriolis Mass Flowmeter with Free Ends", *Flow Measurement and Instrumentation*, vol. 12(5-6), pp. 411 – 420, 2002.

[4] Comet Version 2.00 – User Manual, *Institute of Computational Continuum Mechanics GmbH (ICCM)*, Hamburg, 2001.

[5] J. Kutin, I. Bajsić, "Stability-Boundary Effect in Coriolis Meter", *Flow Measurement and Instrumentation*, vol. 12, pp. 65 – 73, 2001.

Authors: Gregor Bobovnik, B.Sc.; Jože Kutin, M.Sc.; Assoc. Prof. Ivan Bajsić, Ph.D.; University of Ljubljana, Faculty of Mechanical Engineering, Laboratory of Measurements in Process Engineering, Aškerčeva 6, SI–1000 Ljubljana, Slovenia, phone: +386 1 4771 131, fax: +386 1 4771 118, e-mails: gregor.bobovnik@lmps.uni-lj.si, joze.kutin@lmps.uni-lj.si, ivan.bajsic@fs.uni-lj.si.